Melting behavior of single two-dimensional crystal

X. H. Zheng* and R. Grieve
Department of Pure and Applied Physics, The Queen's University of Belfast, Belfast BT7 1NN, United Kingdom
(Received 16 November 2005; published 21 February 2006)

In an experimental system millimeter-sized steel balls repel each other through the Coulomb force to imitate a two-dimensional (2D) atomic lattice in a vacuum both topologically and dynamically. Care has been taken to avoid the formation of grain boundaries. This 2D single crystal melts into a liquid via the hexatic state consistent with the Kosterlitz-Thouless-Halperin-Nelson-Young scenario. Initially in the melting process defects of the 2D lattice tend to emerge from the edge of the crystal. These defects are found to be close to the liquid state according to the Lindemann and Born criteria, confirming the idea of edge melting.

DOI: 10.1103/PhysRevB.73.064205 PACS number(s): 64.70.Dv, 68.90.+g, 41.20.Cv

I. INTRODUCTION

Melting in two dimensions (2D) may serve the purpose of probing the rich details of the melting process in 3D, once envisaged as a single point in the phase diagram without much features.[1–5] To this end we must be careful that the experimental system for 2D melting should possess some important aspects of 3D melting, such as the correlated motion of particles (phonon) and a clearly defined surface of the particle ensemble, etc.

The colloidal suspension system has been used with unparalleled success in helping us to understand 2D melting,[6–9] particularly in terms of the elaborate theory of Kosterlitz, Thouless, Halperin, Nelson, and Young (KTHNY).[10–14] In this theory 2D melting is mediated by defects of the lattice, which is well modeled by the colloidal system topologically. However, other aspects of the lattice—for example, the phonon properties—may be overwhelmed by the viscosity of the colloidal suspension medium. Furthermore, it is apparently difficult to make a single-colloidal-particle crystal with a clear boundary to study the important effect of surface melting[15] [edge melting in 2D (Ref. 1)]. Indeed the experimental evidence has been inconclusive with respect to the KTHNY scenario.[1]

In this communication we study the melting behavior of a single 2D crystal, which is developed in an experimental system capable of modeling both the topological and dynamic properties of a atomic lattice in a vacuum. This crystal is made from millimeter-sized steel balls which repel each other via a Coulomb interaction. The relatively massive balls, compared to the frictional force, make the phonon properties of the system more significant than in the colloidal system.[16–21]

We apply a range of diagnostics, including the Voronoi diagram, the pattern of light scattering, the autocorrelation (g_2) and bond-orientational-correlation (g_6) functions, the local displacement of the balls, and the elastic shear modulus of the crystal, to determine the state of the ball ensemble in our experimental system.[22] We find that the 2D single crystal does melt continuously over a period of temperatures in accordance with the KTHNY scenario. In particular we find clear evidence of the hexatic state, one of the key predictions of the KTHNY theory.

We find that (the first time to our knowledge) particles in topological defects have distinctive dynamic properties. In particular we find that the Lindemann criterion is close to being exceeded in the defects even at the lowest temperature: judged by the Lindemann criterion the particles in the defects in a 2D crystal are always close to being melted. We also find that the defects are mechanically weak: they offer less shear resistivity compared with the bulk, another sign of early melting.

We find that, when the ball ensemble is still in the solid state, the defects tend to emerge from the edge of the 2D crystal, spreading to the interior when temperature increases, giving experimental confirmation of the idea of surface melting. Sometimes the defects form a straight line along one of the crystal vectors, reminiscent a fault line in a crystal. We also find a close correlation in locations between the defects and the so-called Lindemann particles, which mark the melting sites in the crystal.

This communication is arranged as follows. In Sec. II we describe the experimental system. In Sec. III we calibrate the Coulomb force. In Sec. IV we measure the velocity of the balls. In Sec. V we define the reduced temperature and test if the ball ensemble is in thermal equilibrium. We describe the liquid and hexatic states in Secs. VI and VII. We prove that defects tend to gather near the edge of the ball ensemble when it is in the solid state in Sec. VIII. We study the Lindemann and Born criteria in Secs. IX and X. We give brief conclusions in Sec. XI.

II. EXPERIMENTAL SYSTEM

We place millimeter-sized steel balls on a smooth aluminum substrate; both must be thoroughly cleaned first with a chemical solvent and then distilled water. We position an electrically conductive cover above the substrate, which is transparent, allowing us to capture charge-coupled-device (CCD) images, which are processed to let each ball be imaged by a single pixel. The balls start to repel each other when we apply a few thousand volts across the cover and the substrate.[17] The nature of repelling appears to be predominately Coulomb, for the reason that there are net charges on the balls. Indeed when we place an insulating plate beneath the balls, which stops the flux of net charges from the sub-

strate, the repelling force between the balls becomes much weaker. Apparently the dipole interaction, which is the result of charge separation and cannot be stopped by the insulating plate, is dominated by the Coulomb interaction. We adjust this Coulomb interaction to vary the (reduced) temperature of the ball ensemble.

The substrate is rimmed by a hexagonal frame, which also repels the balls, in order for the ball ensemble to develop into a single 2D crystal. The lattice of the ensemble tends to align with the edges of the frame. We find that, when the frame is rectangular, which is incompatible with a hexagonal lattice, a grain boundary (or boundaries) will develop. It is worth mentioning that, even when the frame is hexagonal, the 2D crystal always hosts a few defects (non-six-sided cells in the Voronoi diagram) for the reason that the ensemble does not have the exact number of balls requested by a perfect 2D crystal (7, 19, … and so forth).[20]

The substrate is suspended on a number of strings to allow free horizontal movement. The length of the strings can be adjusted to level the substrate. Sometimes the substrate has to be tilted slightly in order to introduce a gravitational gradient over the ball ensemble to compensate a slight gradient of the Coulomb force, which is the result of electric leakage from the transparent upper electrode via its support or air. We attach a small electric motor to the substrate to drive an eccentric flying wheel to feed kinetic energy into the system. The motor runs at a constant rate in order to avoid complications (for example, resonance) which may take place when the speed of the motor varies.

III. COULOMB FORCE CALIBRATION

In order to calibrate the Coulomb interaction, we place 169 ball bearing balls, 2 mm in diameter, on a square substrate which is leveled in Fig. 1(a) but tilted in Fig. 1(b). For simplicity we assume $f=C/r^2$, where f is the Coulomb force between two balls, separated by a distance r, and C a constant. Therefore, within the constant C, we can calculate f_1 from the locations of the balls, f_1 being the force that deforms the lattice in Fig. 1(b). On the other hand, we know $f_1=mg\sin\theta$, m being the mass of the balls, g gravitational acceleration, and θ angle of substrate inclination: C can be calibrated. We find

$$f = 2\pi\epsilon_0 V^2 \left(\frac{R}{H}\right)^2 \left(\frac{R}{r}\right)^2, \tag{1}$$

which leads to the theoretical values of f_1 in Fig. 1(c). Here R is the radius of the steel ball, H the height of the cover above the substrate, and V the voltage (=8750 V when measuring f). In Eq. (1) the factor of 2 implies that the charges on the ball generate a potential with a value $0.707VR/H$. We can find the same potential between the cover and the substrate at the level $0.707R$ above the substrate; see Fig. 1(c).

In the above measurement we have to know f_2, which is the repelling force between the balls and the confining frame of the substrate. We calculate f_2 in the 169 locations occupied by the balls in Fig. 1(a) on the basis that f_2 and f_1 are balanced when the substrate is leveled. We extrapolate numerically the 169 values of f_2 to the whole interior of the

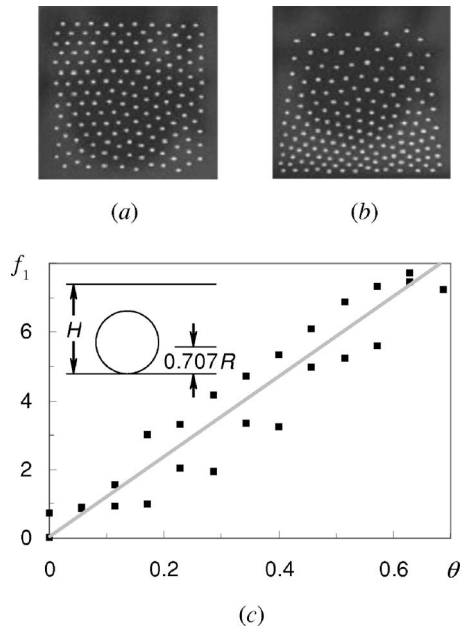

FIG. 1. Coulomb force measurement. (a) The substrate is leveled. (b) The substrate is tilted to deform the particle lattice. (c) Component of gravity force (f_1, in 10^{-6} N) calculated theoretically from deformed lattices at different angles of substrate inclination (θ, in degrees). The calculation is performed twice when θ increases from and returns to 0.

frame in order to know the effect of f_2 when the balls change their locations on the tilted substrate. We find Eq. (1) again in another measurement with balls 5 mm in diameter.

In our melting experiment $H=10$ mm, $R=1$ mm, and V varies between 6.5 and 9.6 kV. According to Eq. (1) and the formula $f=Q^2/4\pi\epsilon_0 r^2$ we have

$$Q = 3.2 \sim 4.8 \times 10^8 e, \tag{2}$$

which can be compared with the rough estimation $10^9 e$ in Ref. 18. We cannot charge the balls much further; otherwise, they will be lifted up from the substrate by the voltage and jump up and down violently. We emphasize that both Eqs. (1) and (2) are associated with our simple model assuming that the balls are point charges in a vacuum. In an alternative model the electrically conductive substrate is seen as a mirror, where each ball has an "image" with equal but opposite charges to weaken the repelling force, so that Q has to become much stronger: charges on a ball must generate a potential $\sim 2.88VR/H$, exceeding the potential at the top of the ball (see Fig. 1) which is apparently unreasonable. In reality Q might be moderately higher than the values in Eq. (2).

IV. VELOCITY DISTRIBUTION

In our experiment the substrate shakes the balls to feed kinetic energy into the system, a method which differs from the natural process of heating. Therefore we must verify if the velocities of the ball are of a Maxwellian distribution in order to simulate the melting process properly. We place 604 balls (2 mm diameter) on a hexagonal substrate and let the motor rotate at 3.43 Hz. Motion of the substrate itself is

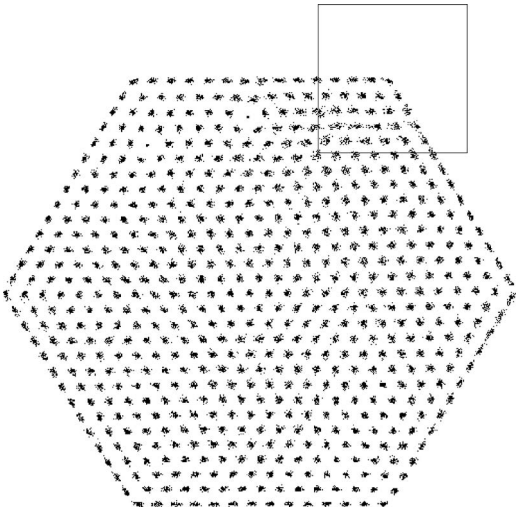

FIG. 2. Traces of 604 balls in an ensemble ($\Gamma=50$). These are found from 50 digitized CCD images taken in ~10 s.

hardly detectable: the image of a ball pinned on the substrate almost always falls into the same pixel (displacement <0.235 mm). We treat the substrate as static in CCD image processing. On the other hand, motion of the balls can be detected easily. We trace the trajectories of each balls from the sequential CCD images (Fig. 2). Then we calculate the velocities of the balls from their displacement and time interval between two images. We find

$$\frac{1}{2}m\langle v^2\rangle = 2.6 \sim 3.7 \times 10^{-10}\ \mathrm{J} \tag{3}$$

when V varies between 6.5 and 9.6 kV, where m and v are the mass and velocity of a ball and the angular brackets stand for ensemble average. In Ref. 18 movement of the balls relative to the substrate is ignored. Instead the balls are assumed to spin like gyros at the rate of the motor shaking the substrate, so that the kinetic energy of a ball is determined by $m\omega^2 d^2/2$, where ω is the angular frequency of shaking, $d=2R$ the ball diameter, giving 1.85×10^{-8} J, and 3.00×10^{-8} J for a ball in Ref. 18 and our experiment, respectively.

In Fig. 3 we plot the theoretical Maxwellian probability together with the experimental result. The mean velocity for the theoretical curve is chosen to be identical to the experimental mean velocity. The experimental data are collected from 50 CCD frames (~34 complete cycles of the driving motor, same V). These data are relatively sparse at low velocities, because with a CCD camera we can only sample the location of a ball as a pixel; i.e., the balls can only move 1, 1.414, 1.732, 2, …, in units of pixels. In general the theory and experiment match closely. There are some discrepancies, notably that the experimental probability does not vanish for static balls, because slow-moving balls may be picked by the CCD camera as static if they are unable to move more than half a pixel in one CCD frame.

V. REDUCED TEMPERATURE

We identify the state of the ball ensemble with the familiar parameter

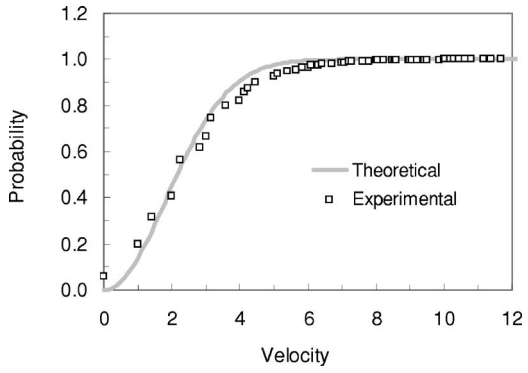

FIG. 3. Theoretical Maxwellian probability and experimental observation, $\Gamma=31$. The velocity is in the unit of pixel/Δt, Δt being the time the CCD camera changes a frame. On average the difference in probability is 0.03 between theory and experiment.

$$\Gamma = \frac{Q^2}{4\pi\epsilon_0 a k_B T}, \tag{4}$$

where a is the ensemble average of r in Eq. (1), k_BT the kinetic energy of a ball, and ϵ_0 the vacuum permittivity. Although Γ is designed for the Coulomb interaction, it is often employed for other interactions.[23] In our experiment $a\simeq4.5$ mm (~19 pixels) which leads through Eqs. (2) and (3) to $\Gamma=50-14$, or $1/\Gamma=0.02-0.07$. We will refer to $1/\Gamma$ ($\neq T$) as the reduced temperature (or temperature for short).

When we assign a single temperature to the ball ensemble to mark its state, we imply that the ensemble is in thermodynamic equilibrium. Therefore we have to verify if Q and k_BT are uniform over the ensemble. In Fig. 4 we show the distribution of the bond length (distance between neighboring balls) from 50 CCD images of the ball ensemble at the same temperature, where the standard deviation of the bond length is ~8%, despite the fact that the balls are constantly agitated by the vibrating substrate. Apparently the repelling force between the balls is fairly uniform, which indicates that Q is uniform.

When the temperature increases, on average the bond length also increases, but only slightly. We see from Fig. 5 that, when Γ is reduced from 50 to 14, the average bond length increases only by 2%. It appears that, although Coulomb repulsion becomes much stronger when we increase the voltage across the substrate and cover by 48%, the repul-

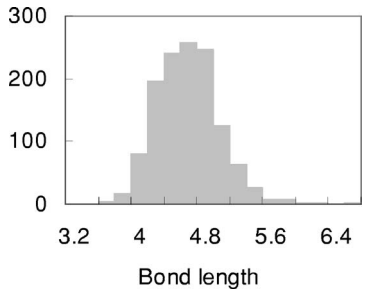

FIG. 4. Histogram of 1271 bonds, collected from 50 CCV images, in the ball ensemble at $\Gamma=50$. On average the bond length is 4.49 mm with standard deviation 0.37 mm (8.2%).

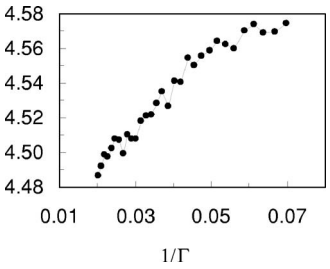

FIG. 5. Bond length (mm) against temperature. At each Γ the bond length is averaged first over the ball ensemble and then over 50 CCD images. The range of variation in bond length is less than 2% when Γ varies between 14 and 50.

sion between the balls and frame of the substrate also becomes much stronger, such that the volume of the ball ensemble remains virtually constant.

We define the mean velocity of the ball as

$$\bar{v}(\mathbf{r}_i) = \frac{1}{50}\sum_{n=1}^{50} v(\mathbf{r}_i, t_n), \tag{5}$$

where the summation is over the 50 sampling moment t_n in ~10 s (~34 complete cycles of the driving motor; see Sec. IV) and $\mathbf{r}_i$ marks the mean coordinates of the balls, $i = 1, 2, \ldots, 604$. We plot $\bar{v}$ as a gray-scale map in Fig. 6 which measure the uniformity of k_BT over the ensemble. There is a ball in each of the Voronoi cells, which are drawn in accordance with the instant coordinates of the balls at a certain moment t_n. Tones of the cells are determined in accordance with the magnitude of $\bar{v}$. It is apparent that most cells are of similar tones; i.e., k_BT is fairly uniform.

VI. LIQUID STATE

We detect the liquid state primarily through the numerically generated pattern of Bragg scattering. We use a program for fast Fourier transform to convert the lattice in real 2D space into a lattice in reciprocal space which resembles closely the pattern of x-ray or electron diffraction from molecular 2D ensembles.[24] It is clear from the upper row in Fig. 7 that in the solid state the scattering pattern is featured with discrete bright spots in a hexagonal array. We identify the liquid state once the scattering pattern is reduced to a few rings without the bright spots, as is shown in the bottom row in Fig 7. The temperature at which the ball ensemble is melted into a liquid can be detected without ambiguity, because the bright spots in the scattering pattern vanish abruptly. This is reflected in Fig. 8, which shows a clear gap between the gray and dashed gray curves of g_6; the latter arise when the bright spots vanish. Indeed these bright spots indicate the existence of bound-orientational order and g_6 is designed to measure it.[22] We find in our experiment the ball ensemble melts into the liquid state when $\Gamma = 22.8$, which is associated with our simple model that the balls are point charges in a vacuum and might become somewhat higher when the presence of the metallic substrate is taken into account; see Sec. III.

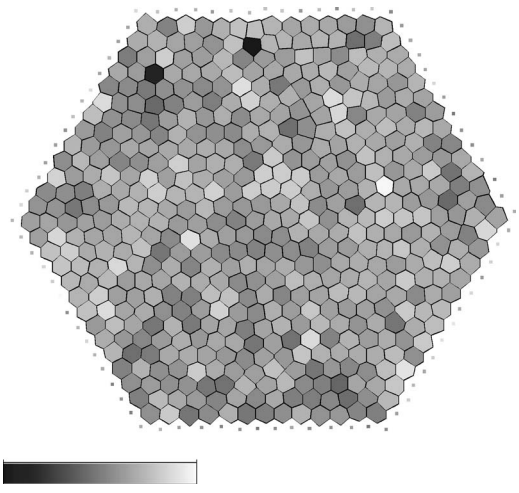

FIG. 6. Gray-scale map of $\bar{v}$ when $\Gamma = 50$ (standard deviation 9.9%); see Eq. (5). Boundary balls are shown as dots, also scaled in accordance with their mean velocity. Grays in the scale bar range from the minimum to maximum values of $\bar{v}$.

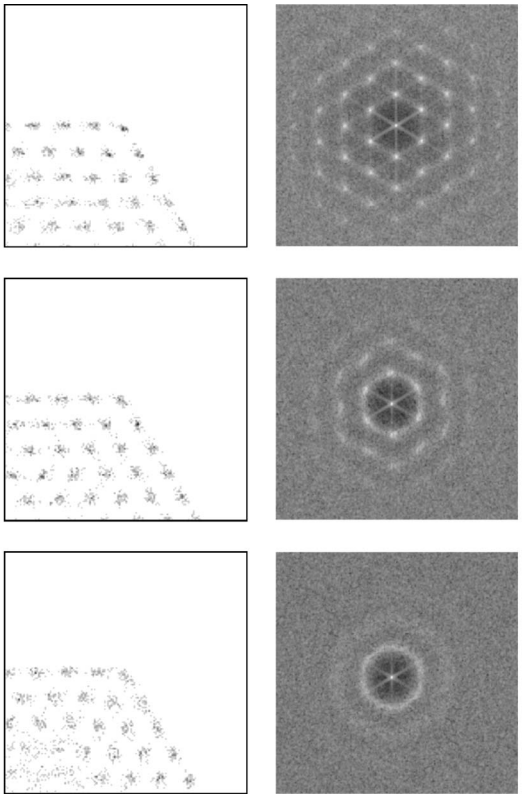

FIG. 7. Enlarged traces of balls and patterns of light scattering for the ensemble of 604 balls shown in Fig. 2: top $\Gamma = 50$ (solid), middle $\Gamma = 28$ (hexatic), and bottom $\Gamma = 18$ (liquid).

In the literature the melting values of Γ for 2D Coulomb crystals vary significantly, ranging from 2.8 (Platzman and Fukukawa, phonon theory), 78.71 (Thouless, defect theory) to 20 700 (Thomas *et al.*, plasma dust experiment).[25–27] In the late 1970s and early 1980s consistent results were found from a number of experiments and simulations. In the experiment by Grimes and Adams[28] a 2D crystal was developed in a sheet of electrons on a liquid He surface, which

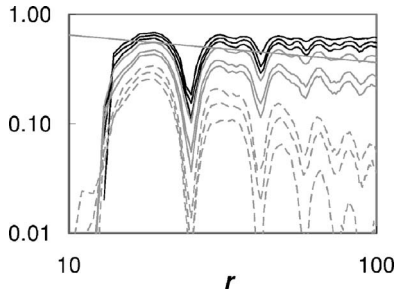

FIG. 8. Bond orientational order correlation function g_6 in logarithm scale, where the distance (r, in pixels) is also in logarithm scale. At each temperature the 50 CCD images give 50 g_6 curves, which are averaged to give the curves in black (solid, $\Gamma=50,40,33$), gray (hexatic, $\Gamma=32,28,24$), and dashed gray (liquid, $\Gamma=23,18,14$). The smooth gray line is a plot of $1.15/r^{1/4}$. Note that the incremental step in Γ is chosen to be small when phase transition takes place to show the rather drastic change in g_6.

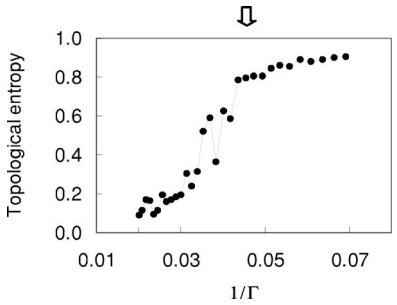

FIG. 9. Topological entropy (in k_B). Melting point indicated by the block arrow.

melts at $\Gamma=137\pm15$.[28] In the Monte Carlo simulation by Gann *et al.* melting takes place at $\Gamma=125\pm15$.[29] In the molecular dynamics simulation by Morf[30] and Kalia *et al.*[31] melting takes place when $125<\Gamma<132$ and $118<\Gamma<130$, respectively. These simulations are designed to imitate the experiment in Ref. 28 closely with respect to for example the effect of viscosity.

It appears that the melting temperature of a 2D Coulomb crystal is related to the experimental condition. In an early simulation by Hockney and Brown, which was performed before the experiment in Ref. 28, the melting value of Γ was found to be 95 ± 2.[32] In the molecular dynamics simulation by Schweigert *et al.* a 2D plasma dust crystal melts at $\Gamma=135$,[33] which is consistent with the results in Refs. 28–31. However, when two such crystals are stacked to form a bilayer, melting takes place at $\Gamma=23$,[33] which is close to our result. In our experiment the substrate can be seen as a mirror, in which each ball has an "image" with opposite charge, in order to neutralize the substrate (grounded in the experiment). Do we actually have a bilayer crystal in our experiment? It will be interesting to find out.

VII. HEXATIC STATE

When $23<\Gamma<33$ the ball ensemble in our experiment is in the so-called hexatic state, which is neither ordered as a solid nor isotropic as a liquid. We see from the middle row of Fig. 7 that the scattering pattern is still featured with a hexagonal array of discrete bright spots, similar to that in the solid state. On the other hand, some of the bright spots have deteriorated into filaments and started to join together to become circular rings, which is most apparent in the second and third shells of the spot array, typical for a liquid state. This feature is also apparent in the pattern of electron diffraction from a liquid-crystal film, which is identified to be in the hexatic state.[24]

It is also apparent from the middle row of Fig. 7 that, in the pattern of light scattering, deterioration of the bright spots becomes more severe the larger the distance from the center. This is reflected in Fig. 8 that in the hexatic state values of g_6 start to drop algebraically when its argument increases. We see that, at $\Gamma=32$, the curve of g_2 is well enveloped by the gray curve proportional to $1/r^{1/4}$ which, according to the KTHNY theory, marks the onset of the hexatic state.

We find that in the hexatic state properties of the ball ensemble vary continuously, in accordance with the KTHNY scenario. These include the number of defects, the local displacement of the balls, and the shear modula, which can be detected by the diagnostics at our disposal. Details will be discussed in the following sections.

VIII. DEFECTS

When the temperature increases, the number of defects (non-six-sided cells) increases continuously in the Voronoi diagram. In order to quantify this trend, we define

$$S=-k_B\sum_n p_n \ln p_n, \tag{6}$$

where k_B is the Boltzmann constant and $p_n=N_n/N$, N_n being the number of n-sided cells and N total number of cells. Equation (6) measures the order of the ball ensemble and is analogues to the expression for entropy per particle. We will refer to S as the topological entropy in the following text. We see from Fig. 9 that the 2D solid melts when $S=0.78k_B$.

In Fig. 10 we show a Voronoi diagram for an ensemble of the balls in the solid state. We do not draw cells around the balls on the edge of the 2D lattice (or edge balls for short). Non-six-sided cells are shaded as defects. Inside the diagram defects cluster into a dipole and a quadripole to allow Burger's vectors to form closed circuits. These arise probably because the number of balls does not equal the exact number requested by a perfect hexagonal 2D crystal; see Sec. II. The single defect on the east corner of the diagram, however, is probably due to thermal agitation.

In Fig. 10 we also show a density map of the defects, which are collected from 50 CCD images at $\Gamma=50$. The shade of the density map is in a gray scale proportional to the overlapping frequency of the defects. It is not difficult to recognize that the quadripoles wander over the interior of the ball ensemble rather freely, with a tendency to be close to the north side. On the other hand, a single defect tends to appear on the east corner, indicating that our experimental system is slightly asymmetric topologically or dynamically.

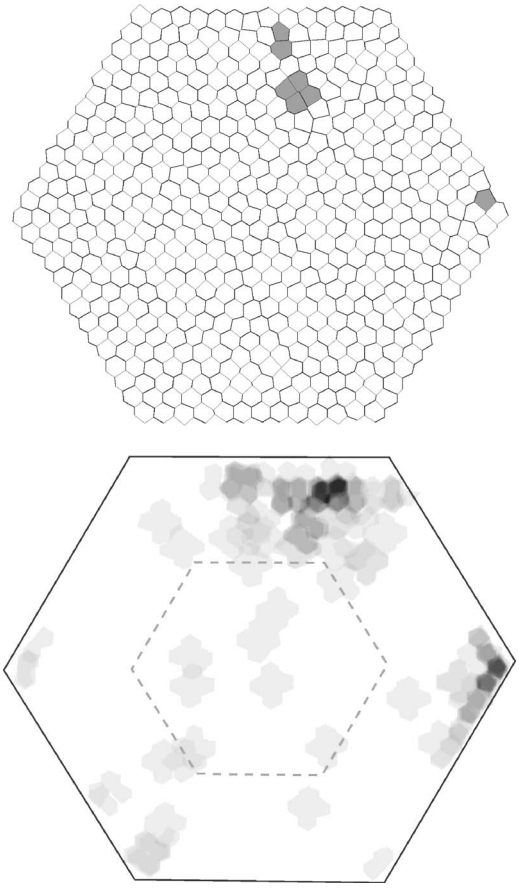

FIG. 10. Defect aggregation at $\Gamma=50$. Top: Voronoi diagram of the ball ensemble, defects shaded. Bottom: density map of all defects in 50 CCD frames, which are collected in ~10 s when the substrate is driven ~35 cycles by the motor.

To quantify our visual impression, we calculate the probability for a pixel to be covered by a defect in 50 sequential CCD images at the same temperature. We average this probability over a series of concentric hexagonal shells with an increasing distance to the crystal boundary (shrinking circumference). One such shell is illustrated as a dashed hexagon in the density map in Fig. 10. Our results are shown in Fig. 11 for $\Gamma=18$ (liquid), 28 (hexatic), and 33 and 50 (solid).

In Fig. 11 the probability curve for defect coverage at $\Gamma=50$ has two peaks at ~26 and 51 pixels inside the edge of the 2D crystal. The first peak is narrower, apparently due to the narrow strip of single defects on the east corner of the density map in Fig. 10. The second peak is broader, apparently due to the quadripoles which tend to gather near the north side of the density map but do not reach the very edge. At $\Gamma=33$ the probability becomes higher for a pixel to be covered by a defect. The probability curve peaks at ~27 pixels inside the crystal edge, which is still in a strip in contact with the edge of the 2D crystal. This peak becomes broader and probably has absorbed the peak due to the quadripoles. However, the trend is unmistakable: defects are most likely to emerge from the edge of the crystal.

We also see from Fig. 11 that, in the hexatic and liquid states, the probability is more or less equal for a pixel to be

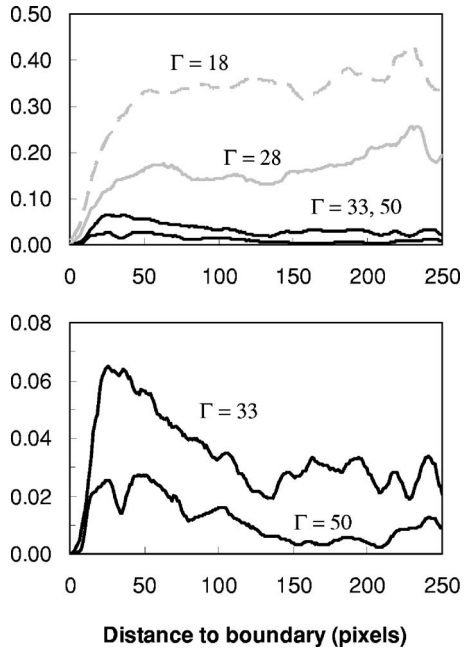

FIG. 11. Probability of defect coverage against distance to the edge of 2D crystal. Upper: solid (black), hexatic (gray), and liquid (dashed gray) states in the same scale. Lower: the scale is changed to show details of the two solid states.

covered by a defect in the density map. The seemingly apparent trend of a higher coverage probability towards the center of the ball ensemble is in fact an illusion. It is easy to understand from the density map in Fig. 10 that, when the dashed hexagon shrinks, it tends to exaggerate the probability of defect coverage, which is the number of defect coverage divided by the number of pixels on the dashed hexagon. This may have also contributed to the rising defect coverage probability towards the center when the ball ensemble is in the solid state.

In Fig. 12 we show density maps of defects in an almost continuous range of temperatures when the ball ensemble is in the solid state. We see that the defects always aggregate near the edge of the 2D crystal and are particularly numerous on the north side of the crystal, probably due to some slight system asymmetry. When $\Gamma=48$ and 46, a number of defects form a straight line, along one of the lattice vectors, to invade the interior of the crystal from the southeast corner, reminiscent of a fault line in a crystal. When $\Gamma=42$ we also see a straight line of defects, along another lattice vector, to link the interior of the crystal to the west corner, although it does not actually reach that corner, probably out of the necessity to form a closed circuit of Burger's vectors.

IX. LINDEMANN CRITERION

The Lindemann criterion states that a solid melts when on average the displacement of its particles exceeds ~10% of the distance between the particles.[34] Bedanov and Gadiyak found through simulation that a 2D solid melts when the displacement of the particles against one of its neighbors exceeds ~30% of the interparticle distance.[35] Zheng and

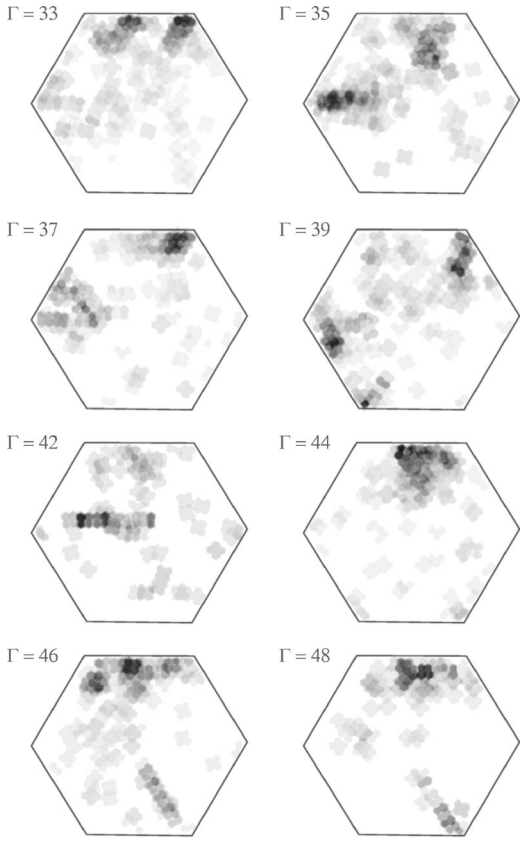

FIG. 12. Density map of defects at various temperatures in the solid state. At each Γ the defects are collected from 50 CCD images in ~10 s when the substrate is driven ~34 cycles by the motor.

Earnshaw found through simulation that, if the displacement is measured in local coordinates, then a 2D solid melts when on average this displacement exceeds ~10% of the interparticle distance.[36] They also used the cooperative motion model[37] to explain the similarity between the melting criteria in 2D and 3D.

Zahn and Maret[38] used a colloidal system to verify the theoretical and simulation results of Zheng and Earnshaw.[36] Now we use our experimental system to verify these results. We define local displacement as the ensemble average of $\mathbf{r}_i(t)-\langle\mathbf{r}_i\rangle_6$, where $i=1,2,\ldots,604$ identifies balls, $\mathbf{r}_i(t)$ marks the instantaneous coordinates of the ith ball, and $\langle\mathbf{r}_i\rangle_6$ the average value of the coordinates of the six or so balls in the first shell surrounding the ith ball.[36] Since this definition of local displacement does not apply to balls on the edge, we exclude the edge balls when we evaluate the local rms displacement over the ball ensemble. Figure 13 shows that the 2D crystal melts when on average the local displacement reaches ~13% of the bond length, which is close to the Lindemann criterion for a bcc lattice in 3D (12.1% of bond length), consistent with the prediction in Ref. 36.

We also find that in defects the local displacement is particularly strong and is in an interesting pattern of development. We see from Fig. 13 that, in the bulk of the ball ensemble, the local displacement is small at low temperatures and grows steadily and quickly when the temperature increases. On the other hand, in the defects, the local displacement is always close to the Lindemann criterion even when the temperature is low. It grows steadily but slowly when the temperature increases. At the melting point the Lindemann criterion is exceeded in both the bulk and defects simultaneously. There is little difference between the bulk and defects with respect to the local displacement at higher temperatures. Apparently, judged with the Lindemann criterion, particles in defects are always close to the liquid state.

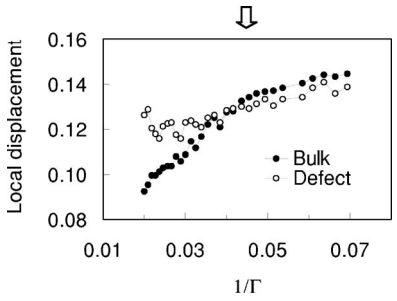

FIG. 13. Values of the rms local displacement of balls (in bond length). The melting point is indicated by the arrow.

According to the cooperative motion model a particle in a 2D solid is in the grip of the shell of its six neighbors.[37] The solid melts because the particle can slip through that shell when the grip of the shell is loosened by thermal agitation. Now we know that, in our experimental system, the movement of a ball is indeed less restricted in a defect, which is a clear indication that the grip the hexagonal lattice is loosened. This justifies the view that particles in defects are close to the liquid state.

We wish to apply the Lindemann criterion to detect the melting sites of the 2D lattice. We identify a Lindemann particle if the local displacement of a ball exceeds 80% of the Lindemann criterion. This definition of Lindemann particle is slightly different from the definition given by Jin *et al.* who identify a Lindemann particle in their 3D simulation if its instantaneous displacement exceeds the Lindemann criterion.[39] However, since the displacement of a particle varies in time, on average the displacement of the Lindemann particle of Jin *et al.* is likely less than the Lindemann criterion; that is, their definition of a Lindemann particle may not be very different from ours. In Fig. 14 we show the traces of the Lindemann particles in our definition when the ball ensemble is in the solid state, which can be compared with the density map of defects in Fig. 12. Apparently there is close correlation in locations between the Lindemann particles and defects. This correlation appears to be worth further exploring from the point of view that melting in 2D may help us to understand melting in 3D: defects play a pivoting role in the KTHNY theory of 2D melting, whereas the Lindemann criterion is applicable in both 2D and 3D.

X. ELASTIC CONSTANT

We derive elastic constants from the statistics of strain fluctuations of the ball ensemble.[40] Strain by definition is associated with a continuum. However, microscopic models for 2D melting are discrete, where strain is not well defined. In the so-called block analysis a series of particle groups

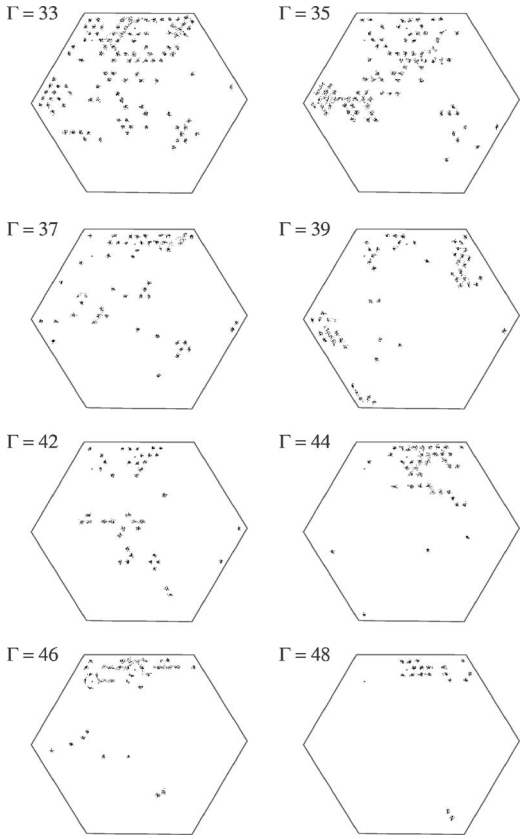

FIG. 14. Traces of Lindemann particles, collected from 50 CCD images at each Γ, which can be compared with the defect maps in Fig. 12.

(blocks), with well-defined free energy, is isolated. Particles in these blocks are sufficiently numerous, so that a relation in the continuum mechanics can be used to relate the free energy with strain. This strain fluctuates when the size of the block varies, giving the elastic constants.[23,41,42] We use a different method of analysis considering the rather limited number of balls in the ensemble. We treat these balls as visible marks on an invisible elastic membrane, where strain is well defined and fluctuates, also giving the elastic constants.

We define $\mathbf{r}_i$ $(i=1,2,\ldots,604)$, which are coordinates of the balls averaged over the 50 CCD images (Fig. 2), as the reference coordinates; see Sec. V. We define $\mathbf{u}_i=\mathbf{r}_i(t)-\mathbf{r}_i$ as the displacement of the ith ball, where $\mathbf{r}_i(t)$ represents the instantaneous coordinates of that ball; see Sec. IX. We link the balls with their nearest neighbors and find an array of triangles; one of them is shown in Fig. 15. In linear approximation we have

$$\mathbf{u}(\mathbf{r}) = A\mathbf{r} + \mathbf{u}_0, \tag{7}$$

where $\mathbf{r}$ and $\mathbf{u}$ are reference coordinates and displacement in a triangle (Fig. 15), A a 2×2 matrix, and $\mathbf{u}_0$ a constant vector with two components. Knowing the values of $\mathbf{u}$ on the tips of the triangle, we can determine both A and $\mathbf{u}_0$. By definition $\epsilon_{11}=\partial u_1/\partial r_1$, $\epsilon_{22}=\partial u_2/\partial r_2$, $\epsilon_{12}=(\partial u_1/\partial r_2 + \partial u_2/\partial r_1)/2$, and ϵ_{ij} are strains, so that

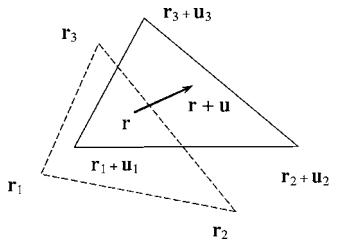

FIG. 15. Reference (dashed line) and instantaneous (solid line) triangles; $\mathbf{r}_i$ and $\mathbf{u}_i$, $i=1,2,3$, are reference coordinates and displacement of balls. In the triangle $\mathbf{r}$ is also displaced by $\mathbf{u}$.

$$\epsilon_{11} = A_{11}, \quad \epsilon_{22} = A_{22}, \quad \epsilon_{12} = (A_{12} + A_{21})/2, \tag{8}$$

which are constant in the triangles, but fluctuate over the ball ensemble. We have

$$S_{33} = \frac{k_B T/\Omega_0}{\langle \Delta\epsilon_{12}\Delta\epsilon_{12}\rangle} \tag{9}$$

as one of the elastic constants, which measures the ability of the material to resist shear, where $\Delta\epsilon_{12}=\epsilon_{12}-\langle\epsilon_{12}\rangle$, the angular brackets denote ensemble average, and Ω_0 is the area of the 2D ensemble. Other elastic constants have similar expressions; see Ref. 41.

We use Eq. (9) to find 50 values of S_{33} from the 50 CCD images at each temperature, which are averaged and plotted in Fig 16. Although the result fluctuates, particularly when the ball ensemble is in the hexatic state, the trend is clear that S_{33} drops continuously when the temperature increases. It is also clear that, when the ensemble is melted into the liquid state, S_{33} drops to a low value and ripples around that low value afterwards, in accordance with the Born criterion that a liquid offers no shear resistivity.[15]

Now we let the angular brackets in Eq. (9) denote the average over the defects instead of the ball ensemble. We compare the resultant S_{33} with its value in the bulk. We see from Fig. 16 that the shear resistivity in defects is always lower than that in the bulk. Apparently the defects are mechanically weaker, compared with the bulk, which is a sign of early melting. Here again the correlation between defects and low shear resistivity is worth further exploring: defects are important in 2D melting, whereas the Born criterion is applicable in both 2D and 3D.

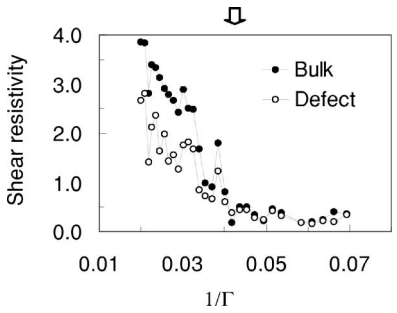

FIG. 16. Shear resistivity measured by S_{33} (in the unit of $k_B T/\Omega_0$). The melting point is indicated by the arrow.

XI. CONCLUSIONS

In 1934 Herzfeld and Mayer argued that in a crystal fusion should occur in channels communicating with the outside; otherwise, the melting crystal cannot be in equilibrium, as the expanded volume of the melt stresses the interior of the lattice locally.[43] If this argument is applicable in 2D, then we should be able to see defects emerge first from the edge of a melting crystal, when particles in the defects are in the liquid state. Conversely we should be able to prove that particles in defects are in the liquid state, when the defects emerge first from the edge of a melting 2D crystal.

In this communication we show that in a single 2D crystal, where measures have been taken to avoid formation of a grain boundary or boundaries, defects do emerge preferably from the edge of the crystal at the early stage of melting. On the other hand, we show that, according to the Lindemann criterion, particles in the defects are always close to be melted even at low temperatures. We also show that, according to the Born criterion, particles in defects behave more like a liquid compared with particles in the bulk as a whole.

In this communication we also show that the single 2D crystal does melt according to the KTHNY scenario. We show through a range of diagnostics that, between the solid and liquid states, the 2D ensemble is in the hexatic state, which is neither ordered as a solid nor isotropic as a liquid. In particular we show that both the population of defects and shear resistivity vary continuously in the hexatic state.

In our experiment the single 2D crystal develops in a system which imitates a 2D atomic lattice in a vacuum both topologically and dynamically. In this system particles interact with each other through the Coulomb interaction, which also imitate charged particles in a vacuum. When analyzing this system, we have adopted a simple model that particles in our experiment are point charges in a vacuum and find a relatively low value of Γ when the 2D ensemble melts into a liquid. Further effort appears to be necessary to study the effect of the metal substrate on the repelling interaction.

Sheng, Lu, and Ma demonstrated that the melting and freezing behaviors of In, Sn, Bi, Cd, and Pb are modified significantly when these metals are milled into nanosized particles and then embedded in an environment of a metal (Al).[44] There have been recent attempts to modify the melting behavior of 2D colloidal crystals by using optical tweezers to pin the particles.[45–47] In the future we will also observe if the melting and freezing behavior of the single 2D crystal in our experiment would be modified when, for example, the edge balls are pinned to the substrate.

*Electronic address: xhz@qub.ac.uk

[1] J. G. Dash, Rev. Mod. Phys. **71**, 1737 (1999).
[2] F. F. Abraham, Phys. Rep. **81**, 339 (1981).
[3] H. Shechter, R. Brener, M. Folman, and J. Suzanne, Phys. Rev. B **41**, 2748 (1990).
[4] R. M. Feenstra, A. J. Slavin, G. A. Held, and M. A. Lutz, Phys. Rev. Lett. **66**, 3257 (1991).
[5] D. B. Pengra and J. G. Dash, J. Phys.: Condens. Matter **4**, 7317 (1992).
[6] C. A. Murray and D. H. Van Winkle, Phys. Rev. Lett. **58**, 1200 (1987).
[7] A. J. Armstrong, R. C. Mockler, and W. J. O'Sullivan, J. Phys.: Condens. Matter **1**, 1707 (1989).
[8] Y. Tang, A. J. Armstrong, R. C. Mockler, and W. J. O'Sullivan, Phys. Rev. Lett. **62**, 2401 (1989).
[9] K. Zahn, R. Lenke, and G. Maret, Phys. Rev. Lett. **82**, 2721 (1999).
[10] J. M. Kosterlitz and D. J. Thouless, J. Phys. C **6**, 1181 (1973).
[11] B. I. Halperin and D. R. Nelson, Phys. Rev. Lett. **41**, 121 (1978).
[12] D. R. Nelson and B. I. Halperin, Phys. Rev. B **19**, 2457 (1979).
[13] A. P. Young, Phys. Rev. B **19**, 1855 (1979).
[14] N. D. Mermin, Phys. Rev. **176**, 250 (1968).
[15] R. W. Cahn, Nature (London) **323**, 668 (1986); **413**, 582 (2001).
[16] G. E. Blonder, Bull. Am. Phys. Soc. **30**, 5403 (1985).
[17] B. Pouligny, R. Malzbender, P. Ryan, and N. A. Clark, Phys. Rev. B **42**, 988 (1990).
[18] B. V. R. Tata, P. V. Rajamani, J. Chakrabarti, Alex Nikolov, and D. T. Wasan, Phys. Rev. Lett. **84**, 3626 (2000).
[19] M. Saint Jean, C. Evan, and C. Guthmann, Europhys. Lett. **55**, 45 (2001).
[20] M. Saint Jean, C. Guthmann, and C. Coupier, Eur. Phys. J. B **39**, 61 (2004).
[21] G. Coupier, C. Guthmann, Y. Noat, and M. Saint Jean, Phys. Rev. E **71**, 046105 (2005).
[22] *Bond-orientational Order in Condensed Matter Systems*, edited by K. J. Strandburg (Springer-Verlag, New York, 1992).
[23] K. Zahn, A. Wille, G. Maret, S. Sengupta, and P. Nielaba, Phys. Rev. Lett. **90**, 155506 (2003).
[24] C-F. Chou, A. J. Jin, S. W. Hui, C. C. Huang, and J. T. Ho, Science **280**, 1424 (1998).
[25] P. M. Platzman and H. Fukuyama, Phys. Rev. B **10**, 3150 (1974).
[26] D. J. Thouless, J. Phys. C **11**, L189 (1978).
[27] H. Thomas, G. E. Morfill, V. Demmel, J. Goree, B. Feuerbacher, and D. Möhlmann, Phys. Rev. Lett. **73**, 652 (1994).
[28] C. C. Grimes and G. Adams, Phys. Rev. Lett. **42**, 795 (1979).
[29] R. C. Gann, S. Chakravarty, and G. V. Chester, Phys. Rev. B **20**, 326 (1979).
[30] R. H. Morf, Phys. Rev. Lett. **43**, 931 (1979).
[31] R. K. Kalia, P. Vashishta, and S. W. de Leeuw, Phys. Rev. B **23**, 4794 (1981).
[32] R. W. Hockney and T. R. Brown, J. Phys. C **8**, 1813 (1975).
[33] V. A. Schweigert, I. V. Schweigert, A. Melzer, A. Homann, and A. Piel, Phys. Rev. Lett. **80**, 5345 (1998).
[34] F. A. Lindemann, Phys. Z. **11**, 609 (1910).
[35] V. M. Bedanov and G. V. Gadiyak, Phys. Lett. **109**, 289 (1985).
[36] X. H. Zheng and J. C. Earnshaw, Europhys. Lett. **41**, 635 (1998).
[37] B. J. Alder, W. G. Hoover, and T. E. Wainwright, Phys. Rev. Lett. **11**, 241 (1963).
[38] K. Zahn and G. Maret, Phys. Rev. Lett. **85**, 3656 (2000).
[39] Z. H. Jin, P. Gumbsch, K. Lu, and E. Ma, Phys. Rev. Lett. **87**, 055703 (2001).
[40] L. D. Landau and E. M. Lifshitz, *Theory of Elasiticity*, 3rd ed.

(Pergamon, Oxford, 1986).
[41] M. Parrinello and A. Rahman, J. Chem. Phys. **76**, 2662 (1982).
[42] S. Sengupta, P. Nielaba, M. Rao, and K. Binder, Phys. Rev. E **61**, 1072 (2000).
[43] K. F. Herzfeld and M. G. Mayer, Phys. Rev. **46**, 995 (1934).
[44] H. W. Sheng, K. Liu, and E. Ma, Acta Mater. **46**, 5195 (1998).
[45] M. Brunner and C. Bechinger, Phys. Rev. Lett. **88**, 248302 (2002).
[46] K. Mangold, P. Leiderer, and C. Bechinger, Phys. Rev. Lett. **90**, 158302 (2003).
[47] C. Reichhardt and C. J. Olson Reichhardt, Phys. Rev. Lett. **92**, 108301 (2004).